Excitonic States in Cylindrical Quantum Dots: A Variational Approach

Author: Saad Boulaich Marso
Facultat de Física, Universitat de Barcelona, Diagonal 645, 08028 Barcelona, Spain.

Advisor: Amílcar Labarta Rodríguez

Abstract: This work studies the exciton ground-state energy in a cylindrical quantum dot using a variational method. A trial wavefunction incorporating both in-plane and vertical confinement effects is employed to study the energy as a function of radius R and height H. The study also includes a detailed comparison between the 2D disk and 3D sphere geometries, using an identical trial wavefunction. Results show that quantum confinement dominates at small sizes, an optimal aspect ratio $R/H \approx 0.53$ exists, and the correlation energy decreases with increasing system size.

Keywords: Quantum confinement, Exciton, Variational method, Semiconductor quantum dots, Cylindrical geometry, Coulomb interaction.
SDGs: Quality education (Educació de qualitat), Net and sustainable energy (Energia neta i sostenible).

I. INTRODUCTION

In 1937, Herbert Fröhlich predicted the emergence of quantum size effects at nanometric scales and low temperatures. These effects are particularly pronounced in semiconductors, where the low effective mass of electrons enhances the de Broglie wavelength and confinement effects [1].

Quantum dots (QDs) that are nanometric particles of a semiconductor lie at the core of nanoscience due to the strong size and composition dependence of their physical and optical properties. Unlike bulk materials, they exhibit discrete energy levels and tunable bandgaps, behaving as particles (electrons and holes) confined in a potential well. Their unique behavior stems from their intermediate scale between molecular and bulk regimes [1, 2].

Advancements in thin-film electronics, especially through molecular beam epitaxy (MBE), enabled the fabrication of GaAs quantum wells within AlGaAs barriers. Combined with techniques like mass spectrometry and substrate etching, MBE allowed direct observation of discrete quantum states and high-resolution heterostructures. However, these structures remained embedded in bulk matrices, limiting the realization of true quantum confinement [1].

The first experimental identification of QDs came in 1979, when Yekimov and collaborators observed semiconductor nanocrystals in Cu- and Cl-doped silicate glasses. Heat treatment at 4.2 K yielded absorption spectra similar to crystalline CuCl[3]. Small-angle X-ray scattering revealed nanocrystals with tunable sizes from a few to several tens of nanometers. The observed blue shift in the absorption spectrum with decreasing size confirmed the presence of quantum size effects[1].

These effects can be approximated as:

$$\hbar\omega = E_g - E_{\mathrm{ex}} + \frac{\hbar^2\pi^2}{2Ma^2} \tag{1}$$

where E_g is the bulk bandgap of the semiconductor, E_{ex} the exciton binding energy of the electron-hole pair, M their reduced mass, and a the nanocrystal size (see energy scheme in Fig. 1). Accurate estimates of M via self-consistent calculations with Gaussian basis sets have validated the confinement model and explained experimental spectra in the weak-confinement regime.

In 1983, Brus et al. synthesized colloidal CdS QDs stabilized by a copolymer, initially around 4.5 nm. These particles were later recrystallized into larger 12.5 nm crystallites via Ostwald ripening. UV-Vis absorption spectroscopy showed that while larger particles resembled bulk CdS, smaller ones exhibited a blue shift and exciton broadening—hallmarks of size-dependent quantum effects. Brus modeled these using the effective-mass approximation, a spherical potential, and dielectric polarization [4].

Modern QD synthesis relies mainly on liquid-phase colloidal methods, allowing precise control over size, shape, and composition by tuning precursors, surfactants, temperature, and reaction time. Techniques like hot injection, solvothermal growth, and template-assisted synthesis enable scalable production for applications in optoelectronics, bioimaging, photovoltaics, and quantum computing [5].

In semiconductor QDs, the fundamental physical system is the exciton: a Coulomb interacting electron–hole pair formed when an electron absorbs energy exceeding the bandgap E_g, leaving behind a positively charged hole. As the dot size approaches the effective Bohr radius of the atom-like pair, confinement drastically modifies exciton dynamics [6, 7].

Anisotropic QDs, often modeled as cylindrical or disk-like geometries, exhibit enhanced confinement compared to spherical microcrystallites. This strengthens electron–hole Coulomb interactions, stabilizing excitons at room temperature and making them visible in both absorption and emission spectra, which are key features for device applications.

In this work, we model an anisotropic QD as a infinite cylindrical potential well confining an exciton. We compute the ground-state energy using a variational method applied to an effective Hamiltonian including kinetic energy, confinement potentials, and Coulomb attraction. To simplify the analysis, we adopt a separable approximation treating the in-plane (disk) and vertical (z-axis) confinements independently, with simplified wavefunctions for each dimension. The accuracy of this approximation is tested against cases using uncorrelated exact solutions for the two independent particles, showing good agreement and confirming model's validity.

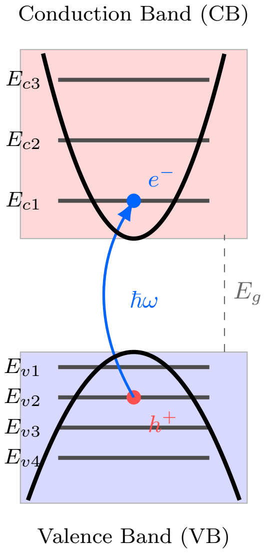

FIG. 1: Schematic representation of quantized energy levels in a QD. The valence band (VB) and conduction band (CB) exhibit discrete states due to quantum confinement, with narrower level spacing in the VB (reflecting heavier hole effective mass, m_h^*) compared to the CB (lighter electron effective mass, m_e^*). The formation of an exciton (e^--h^+ pair) is shown.

II. THEORETICAL DESCRIPTION

We consider an exciton confined within an isolated, cylindrical semiconductor QD of radius R and height H (see Fig. 2). Owing to the symmetry and material properties, we assume isotropic and non-degenerate energy bands. Furthermore, the surrounding material is assumed to possess a sufficiently large band gap, justifying the approximation of the confinement potential as infinite.

A. Coordinate System and Hartree Units

The effective Hamiltonian describing the system reads:

$$\hat{H} = \underbrace{-\frac{\hbar^2}{2m_e^*}\nabla_e^2}_{T_e} \underbrace{-\frac{\hbar^2}{2m_h^*}\nabla_h^2}_{T_h} \underbrace{-\frac{e^2}{4\pi\epsilon|\vec{r}_e - \vec{r}_h|}}_{V_{eh}} \tag{2}$$

where e is the elementary charge, ϵ is the dielectric constant of the medium, and m_e^*, m_h^* are the effective masses of the electron and the hole, respectively. Cylindrical coordinates used to locate the two particles are shown in Fig. 2.

To simplify the analysis, we express all quantities in terms of effective atomic units (Hartree units), where the characteristic length and energy scales are defined as:

$$a_0^* = \frac{4\pi\epsilon\hbar^2}{\mu e^2} \quad \text{(effective Bohr radius)},$$

$$E_h^* = \frac{e^2}{4\pi\epsilon a_0^*} = \frac{\mu e^4}{(4\pi\epsilon)^2\hbar^2} \quad \text{(effective Hartree energy)},$$

with $\mu = \frac{m_e^* m_h^*}{m_e^* + m_h^*}$ being the reduced mass of the electron–hole pair. In these units, the fundamental constants are normalized as $e = \hbar = 1/4\pi\epsilon = 1$. Introducing the mass ratio $\sigma = m_e^*/m_h^*$, the Hamiltonian simplifies to:

$$\hat{H} = -\frac{1}{2(1+\sigma)}\nabla_e^2 - \frac{\sigma}{2(1+\sigma)}\nabla_h^2 - \frac{1}{|\vec{r}_e - \vec{r}_h|} \tag{3}$$

To convert results to SI units, it suffices to multiply lengths by the effective Bohr radius a_0^* and energies by the effective Hartree E_h^*.

The adopted approximation allows for a geometric separation of the system into a two-dimensional disk, characterized by the radial coordinates r_e and r_h (the distances of the electron and hole from the center, respectively), and the in-plane separation r_{eh}, along with a one-dimensional vertical coordinate for each particle, z_e and z_h, as illustrated in Fig. 2.

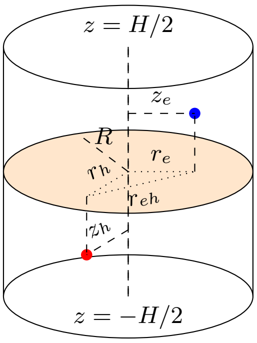

FIG. 2: Schematic representation of the coordinate system for the electron-hole pair in the cylindrical QD. The electron is shown in blue, and the hole in red.

To compute the area element associated with the disk, we start from the geometrical relation $r_{eh} = \sqrt{r_e^2 + r_h^2 - 2r_e r_h \cos(\theta_e - \theta_h)}$ in polar coordinates. Transforming the coordinates, the resulting area element is:

$$dA = 8\pi \frac{r_e r_h r_{eh} dr_e dr_h dr_{eh}}{\sqrt{|((r_e + r_h)^2 - r_{eh}^2)(r_{eh}^2 - (r_e - r_h)^2)|}} \tag{4}$$

For the vertical coordinates, $dZ = dz_e\, dz_h$, leading to a geometric separation between the in-plane and vertical coordinates.

B. Variational Method

The main objective of this work is to determine the ground-state energy of an exciton confined in a cylindrical QD as a function of the radius R and height H. According to the Rayleigh–Ritz variational principle, given a normalized trial wavefunction $|\Phi\rangle$ depending on a variational parameter α, the approximate ground-state energy is obtained by minimizing the energy functional:

$$E(\alpha) = \frac{\langle\Phi|\, H\, |\Phi\rangle}{\langle\Phi|\Phi\rangle}. \tag{5}$$

The value α_0 that minimizes $E(\alpha)$ provides the best upper bound to the true ground-state energy E_0 within the limitations of the chosen trial wavefunction $|\Phi\rangle$ [8]. All Hamiltonian expectation values are normalized with the corresponding integral:

$$\langle\Phi|\Phi\rangle = \iiint_V \Phi^2\, d\tau \tag{6}$$

C. Hamiltonian Expectation Value

Given a trial wave function $|\Phi\rangle$, the kinetic energy operators T_e and T_h can be reformulated by exploiting the Hermiticity of the Laplacian operator and the boundary conditions imposed by strong spatial confinement. Under the assumption that Φ vanishes at the boundaries of the integration domain (consistent with hard-wall confinement) the following general identity holds:

$$\iiint_V \langle\Phi|\, \nabla_e^2\, |\Phi\rangle\, d\tau = -\iiint_V (\vec{\nabla}_e\Phi)\cdot(\vec{\nabla}_e\Phi) d\tau \tag{7}$$

Accordingly, the expectation value of the Hamiltonian restricted to the disk, $\hat{H}_D$, expressed in the chosen coordinate system for a disk and a sphere (see Appendix B), becomes:

$$\begin{aligned}\langle\Phi_D|\, \hat{H}_D\, |\Phi_D\rangle = {} & \frac{1}{2(1+\sigma)}\iiint_D \Bigg\{ \left(\frac{\partial\Phi_D}{\partial r_e}\right)^2 + \left(\frac{\partial\Phi_D}{\partial r_{eh}}\right)^2 + \\ & \left(\frac{\partial\Phi_D}{\partial r_e}\right)\left(\frac{\partial\Phi_D}{\partial r_{eh}}\right)\frac{r_e^2-r_h^2+r_{eh}^2}{r_e r_{eh}}\Bigg\} d\tau + \frac{\sigma}{2(1+\sigma)} \\ & \iiint_D \Bigg\{ \left(\frac{\partial\Phi_D}{\partial r_h}\right)^2 + \left(\frac{\partial\Phi_D}{\partial r_{eh}}\right)^2 + \left(\frac{\partial\Phi_D}{\partial r_h}\right)\left(\frac{\partial\Phi_D}{\partial r_{eh}}\right) \\ & \frac{r_h^2-r_e^2+r_{eh}^2}{r_h r_{eh}}\Bigg\} d\tau - \iiint_D \frac{\Phi_D^2 d\tau}{r_{eh}}\end{aligned} \tag{8}$$

Both cases differ in the differential element $d\tau$. For the disk $d\tau$ is given by Eq. 4, while for the sphere $d\tau = 8\pi^2\, r_e\, r_h\, r_{eh}\, dr_e\, dr_h\, dr_{eh}$. The first two integrals yield equal contributions due to the identical integration domains, namely: $0 \le r_e, r_h \le R$, $|r_e - r_h| \le r_{eh} \le r_e + r_h$. Consequently, they can be combined, leading to an expression for the energy expectation value that is independent of the effective masses of the charge carriers:

$$\begin{aligned}\langle\Phi_D|\, \hat{H}_D\, |\Phi_D\rangle = {} & \frac{1}{2}\iiint_D \Bigg\{ \left(\frac{\partial\Phi_D}{\partial r_e}\right)^2 + \left(\frac{\partial\Phi_D}{\partial r_{eh}}\right)^2 + \\ & \left(\frac{\partial\Phi_D}{\partial r_e}\right)\left(\frac{\partial\Phi_D}{\partial r_{eh}}\right)\frac{r_e^2-r_h^2+r_{eh}^2}{r_e r_{eh}}\Bigg\} d\tau - \iiint_D \frac{\Phi_D^2 d\tau}{r_{eh}}\end{aligned} \tag{9}$$

The general cylindrical configuration will be addressed by properly introducing the vertical coordinate integration.

III. DISCUSSION OF RESULTS

In this section, different confinement geometries are considered: a disk, a sphere, the general cylindrical case, and a discussion of the effects of the cylinder aspect ratio. In each case, a trial wave function without nodes is used that vanishes at the boundaries and peaks at the system center, since we are aiming at guessing the energy of the ground state. The variational ground state energy is computed as a function of R (and H where applicable), with results obtained numerically using *Wolfram Mathematica* [9].

A. 2D Disk and 3D Sphere

A comparison between the 2D disk and the 3D sphere is particularly meaningful, as both geometries are characterized by the same set of variables, r_e, r_h, and r_{eh}. This allows the use of an identical trial wave function in both cases, facilitating a direct comparison of the corresponding ground-state energies.

The exact eigenfunctions of the two particles confined within the disk and without Coulomb interactions (uncorrelated solutions), are Bessel functions of first kind (see Appendix C), given by $J_m(kr)$ (J_0 for ground-state solution), where r is the radial coordinate and k is a constant determined by the system's boundary conditions: vanishing at the boundary, $r_i = R$ (infinite confinement), and presenting a maximum at the origin, $r_i = 0$. That is,

$$\Phi_B = J_0\left(\frac{\theta_0}{R} r_e\right) J_0\left(\frac{\theta_0}{R} r_h\right) \exp\left(-\alpha\ r_{eh}^2\right) \tag{10}$$

where $\theta_0 = 2.4048255577$ is the first zero of the corresponding Bessel function. The Gaussian form term is added to the product of uncorrelated solutions to ensure short-range electron-hole correlation while preserving the required symmetry and boundary conditions. The parameter α serves as a variational parameter to be optimized. Since numerical calculations involving Bessel functions are computationally expensive, we propose the following trial wave function as a more efficient alternative aimed at reducing computation time. This function exhibits linear confinement behavior:

$$\Phi_D = \left(1 - \frac{r_e}{R}\right)\left(1 - \frac{r_h}{R}\right) \exp\left(-\alpha\ r_{eh}^2\right) \tag{11}$$

However, we need to verify its validity by comparing the minimal energies obtained with those given by Eq.10 for the disk.

The close agreement between the results for the Bessel and linear trial wave function curves in Fig. 3 for the case of the disk supports the validity of the proposed ansatz, with the variational parameter minimized at $\alpha_0 = 2.0\, a_0^{*-2}$. Regarding the comparison between the disk and the sphere, the asymptotic ground-state energies for large R differ due to the distinct dimensionality of the system: $E_0^D \approx -2.0\, E_h^*$ for the disk and $E_0^S \approx -0.5\, E_h^*$ for the sphere, which correspond to the ground state of the excitonic hydrogen atom-like in 2D and 3D, respectively. The dimensionality affects the ground-state energy because in lower dimensions the system is more confined, leading to stronger binding and thus more negative ground-state energy.

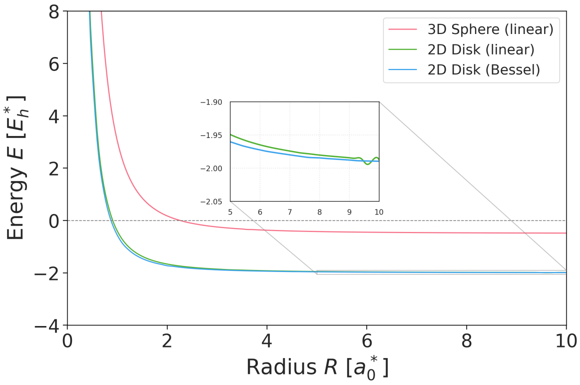

FIG. 3: Ground-state energies obtained variationally as a function of the parameter α for different radii R in both disk (both linear and Bessel wave functions) and sphere.

The divergence toward positive values as $R \to 0$, that is, when the system size becomes much smaller than the Bohr radius, is caused by the increasing kinetic energy due to confinement of both particles, which outweighs the attractive Coulomb interaction between them.

B. Cylindrical System

For the case of the cylinder, the vertical coordinates z_e and z_h are independent in the kinetic term, they must be carefully treated in the Coulomb interaction. For this reason, and to remain consistent with the separable nature of the model, the total Hamiltonian can be separated into the disk contribution, $\hat{H}_D$, given by Eq. 9, and a vertical contribution, $\hat{H}_Z$ ($\hat{H} \approx \hat{H}_D + \hat{H}_Z$). However, the Coulomb term in $\hat{H}_Z$ must retain a functional dependence on the in-plane interaction to properly account for the geometrical correlation inherent to the system. Similarly, the total wave function is separated into an in-plane component Φ and a vertical component Φ_Z ($\Phi \approx \Phi_D \cdot \Phi_Z$), reflecting the approximate separability of the Hamiltonian:

$$\langle \Phi_Z | \hat{H}_Z | \Phi_Z \rangle = \frac{1}{2} \iint_Z \left\{ \left(\frac{\partial \Phi_Z}{\partial z_e} \right)^2 + \left(\frac{\partial \Phi_Z}{\partial z_h} \right)^2 dz_e dz_h - \right.$$
$$- \iint_Z \frac{\Phi_Z^2}{-\frac{N_D}{V_D} + |z_e - z_h|} dz_e dz_h \tag{12}$$

Where $N_D = \iiint_D \Phi^2 dA$, and $V_D = \iiint_D -\frac{\Phi^2}{r_{eh}} dA$. The integration limits are $-H/2 \leq z_e, z_h \leq H/2$. The Coulomb interaction term in the last integral incorporates an approximation that enables the separation of the integrations into in-plane and vertical coordinates. The exact form involves an integral that depends on all geometric variables of the system, resulting in a fivefold integral, and the approximation thus significantly simplifies the calculation [7].

This formulation is physically consistent: when the disk radius R is sufficiently large, we have $|z_e - z_h| \ll \frac{N_D}{V_D}$, and the in-plane (disk) interaction dominates the Coulomb term. Conversely, for $|z_e - z_h| \gg \frac{N_D}{V_D}$, the disk contribution to the vertical Coulomb interaction becomes negligible, and the interaction is effectively governed by the vertical separation between particles. Therefore, the total energy of the system to be minimized is given by:

$$E(\alpha) = \frac{\langle \Phi_D | \hat{H}_D | \Phi_D \rangle}{\langle \Phi_D | \Phi_D \rangle} + \frac{\langle \Phi_Z | \hat{H}_Z | \Phi_Z \rangle}{\langle \Phi_Z | \Phi_Z \rangle} \tag{13}$$

The Coulomb interaction acquires physical meaning when expressed in terms of the distance between particles, for instance with the squared distance $|\vec{r}_e - \vec{r}_h|^2 = r_{eh}^2 + (z_e - z_h)^2$ between particles. To ensure this consistency, a single variational parameter α is used in both trial functions Φ_D and Φ_Z.

The confinement along the vertical direction corresponds to a one-dimensional infinite potential well, whose uncorrelated ground-state solutions for each particle are $\Phi_C \propto \cos\left(\frac{\pi z_i}{H}\right)$ (where i denotes e or h). Thus, the boundary conditions required are analogous to those of Φ_D. To better approximate the cosine profile, we adopt a parabolic approximation for the vertical wave function. This approximation, like the use of Bessel functions, simplifies the numerical computation time significantly:

$$\Phi_Z = \left(\frac{H^2}{4} - z_e^2 \right) \left(\frac{H^2}{4} - z_h^2 \right) \exp\left(-\alpha\, (z_e - z_h)^2 \right) \tag{14}$$

In order to capture the effect of the Coulomb interaction in the system, we define the correlation energy as:

$$E_{\mathcal{W}} = E(\alpha_0) - \frac{1}{2} \left[\left(\frac{\theta_0}{R} \right)^2 + \left(\frac{\pi}{H} \right)^2 \right] \tag{15}$$

where the second term corresponds to the exact kinetic energy for the uncorrelated solution [7].

Maintaining the same Φ_D as in Eq. 11, we compute the correlation energies by fixing specific values of the height H and minimizing the variational parameter α for different values of the radius R. To assess the validity of the chosen trial functions, we perform the same minimization procedure for the case $H = 5a_0^*$, this time using Φ_B for the disk contribution and $\Phi_C = \cos\left(\frac{\pi z_i}{H}\right)$ for the vertical part.

The convergence values of the correlation energy curves (see Fig.4) correspond to the ground-state energy that would be obtained applying Eq.13, because for large radii the Coulomb interaction dominates over confinement effects. Decreasing the height leads the system toward the disk-like regime, while increasing it brings the behavior closer to the spherical case. For instance, for $H = 5\,a_0^*$, the energy value $E_{\mathcal{W}} \approx -0.48$ is very close to that of the sphere. It is also shown that the proposed trial wave functions yield results in close agreement with the corresponding exact uncorrelated solutions.

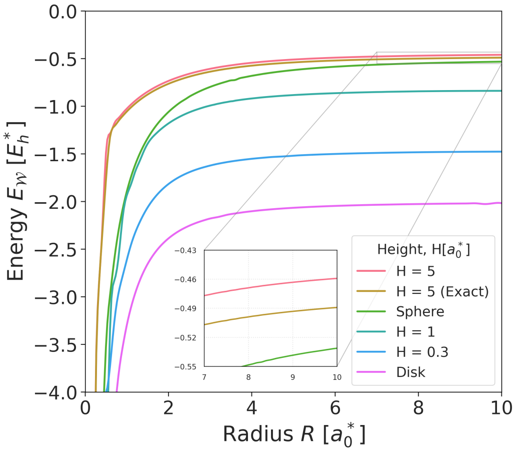

FIG. 4: Correlation energies vs. radius R for different heights H. Inset highlights convergence region. Results use trial wavefunction from Eq. 14 with optimized α. The correlation energy for the disk and the sphere is also included, obtained by subtracting the corresponding uncorrelated kinetic energy from the ground-state energy in each case.

Finally, keeping the volume fixed, $V = \pi R^2 H$, the effect of anisotropy on the ground-state energy is shown in Fig.5 by varying the aspect ratio R/H. In all cases, the variational energy shows a clear minimum near $R/H \approx 0.53$, indicating a preference for similar in-plane and vertical sizes (optimal balance between radial and axial confinement).

In Fig. 5, the curve shapes arise because increasing the aspect ratio R/H reduces the height H relative to the radius R, enhancing vertical confinement and thus increasing the ground-state energy. When the aspect ratio approaches zero, the radius R becomes smaller, intensifying radial confinement and similarly raising the energy.

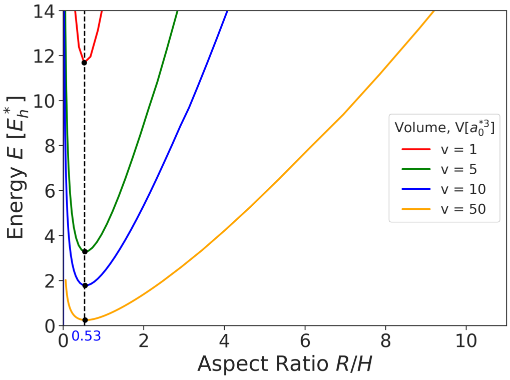

FIG. 5: Variational ground-state energy as a function of the aspect ratio R/H for different fixed volumes V (in units of a_0^{*3}) under cylindrical confinement.

IV. CONCLUSIONS

Ground state energies obtained with simplified trial wavefunctions agree well with the corresponding ones for more complex uncorrelated solutions, validating their applicability. Quantum confinement dominates at small sizes ($R, H \ll a_0^*$), inducing strong energy quantization, while for large systems, the energy approaches the unconfined exciton limits: $-2.0\,E_h^*$ (disk) and $-0.5\,E_h^*$ (sphere). For cylinders, the correlation energy $E_{\mathcal{W}}$ converges to these same asymptotic values at large radii, as Coulomb interactions overcome confinement. Increasing H shifts the system from disk-like toward spherical behavior. The anisotropic study reflects that for an aspect ratio $R/H \approx 0.53$, shapes with similar radial and vertical sizes minimize the ground state energy. Increasing R/H enhances vertical confinement, while decreasing it strengthens radial confinement (raising energy in both cases).

Acknowledgments

I would like to express my deepest gratitude to Professor Amílcar Labarta for his dedication, commitment, and support throughout the entire process of this work, and to my parents, my family, and my friends in Tangier for their moral support over my academic journey.

[1] The Nobel Committee for Chemistry, *Quantum dots — seeds of nanoscience* (NobelPrize.org).
[2] F. Duan and X. Feng, *Introduction to Condensed Matter Physics*, (World Scientific Publishing Company, Singapore, 2005, 5th ed.).
[3] L. Kleinman and K. Mednick, "Energy bands and effective masses of CuCl," *Phys. Rev. B* **20**, 6 (1979).
[4] Y. Wang and N. Herron, *Quantum size effects on the exciton energy of CdS clusters*, Phys. Rev. B **42**, 7253 (1990).
[5] V. Lesnyak, M. Yarema, and S. Miao, *Editorial: Colloidal Semiconductor Nanocrystals: Synthesis, Properties, and Applications*, Chem. Mater. **31**, 9126–9127 (2019).
[6] Y. Kayanuma, "Quantum-size effects of interacting electrons and holes in semiconductor microcrystals with spherical shape," *Phys. Rev. B* **38**, 14 (1988).
[7] S. I. Goff and B. Stebe, "Influence of longitudinal and lateral confinements on excitons in cylindrical quantum dots of semiconductors" *Phys. Rev. B* **47**, 3 (1993).
[8] F. Salvat, *Mecánica cuántica*, (2023, Paperback edition).
[9] Wolfram Research, *Mathematica, Version 14.2*, (, 2025).

Estats excitònics en punts quàntics cilíndrics: un enfocament variacional

Author: Saad Boulaich Marso
Facultat de Física, Universitat de Barcelona, Diagonal 645, 08028 Barcelona, Spain.

Advisor: Amílcar Labarta Rodríguez

Resum: Aquest treball estudia l'energia de l'estat fonamental de l'excitó en un punt quàntic cilíndric utilitzant un mètode variacional. S'empra una funció d'ona de prova que incorpora els efectes de confinament tant en pla com en la direcció vertical per analitzar l'energia en funció del radi R i láltura H. Léstudi inclou una comparació detallada entre les geometries del disc 2D i l'esfera 3D, utilitzant la mateixa funció dóna de prova. Els resultats mostren que el confinament domina en sistemes de mida petita, que existeix una relació òptima d'aspecte $R/H \approx 0.53$, i que l'energia de correlació disminueix amb l'augment de la mida del sistema.

Paraules clau: Confinament quàntic, Excitó, Mètode variacional, Punts quàntics semiconductors, Geometria cilíndrica, Interacció de Coulomb.

ODSs: Educació de qualitat, Energia neta i sostenible

Objectius de Desenvolupament Sostenible (ODSs o SDGs)

1. Fi de la es desigualtats		10. Reducció de les desigualtats	
2. Fam zero		11. Ciutats i comunitats sostenibles	
3. Salut i benestar		12. Consum i producció responsables	
4. Educació de qualitat	X	13. Acció climàtica	
5. Igualtat de gènere		14. Vida submarina	
6. Aigua neta i sanejament		15. Vida terrestre	
7. Energia neta i sostenible	X	16. Pau, justícia i institucions sòlides	
8. Treball digne i creixement econòmic		17. Aliança pels objectius	
9. Indústria, innovació, infraestructures			

GRAPHICAL ABSTRACT

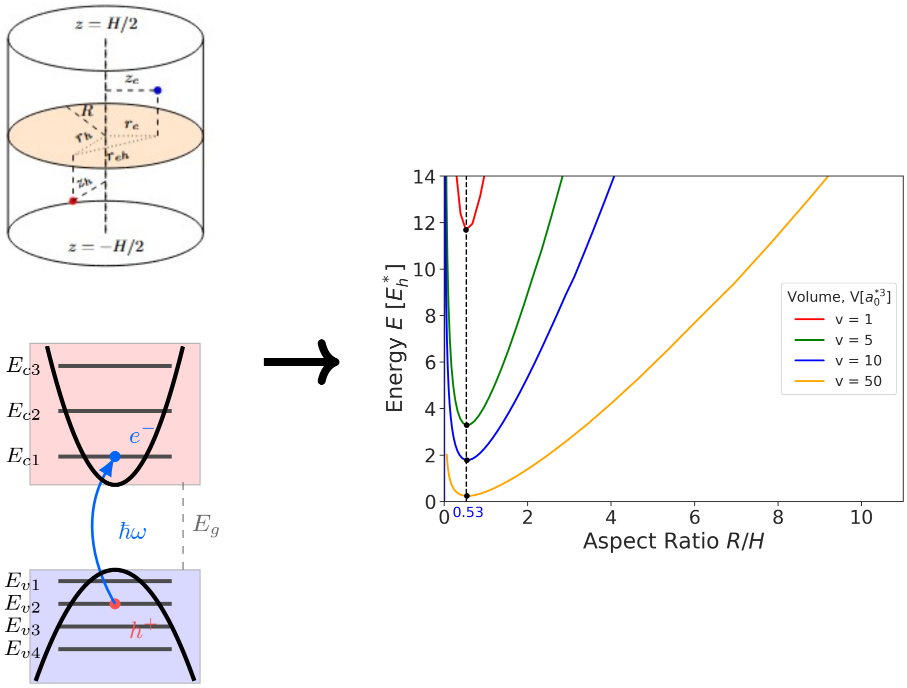

Appendix A: Deduction of Differential Elements

1. Bi-dimensional Disk

In polar coordinates, the in-plane positions of the electron and hole are given by:

$$\vec{r_i} = (r_i, \theta_i), \quad i = e, h \tag{A1}$$

To perform the coordinate change $(r_e, \theta_e, r_h, \theta_h) \to (r_e, r_h, r_{eh})$, we express r_{eh} using the law of cosines:

$$r_{eh} = \sqrt{r_e^2 + r_h^2 - 2r_e r_h \cos(\theta_e - \theta_h)} \tag{A2}$$

Defining $\theta_{eh} \equiv \theta_e - \theta_h$, the differential area element in polar coordinates becomes:

$$dA = 8\pi\, r_e r_h\, dr_e\, dr_h\, d\theta_{eh} \tag{A3}$$

We now apply the chain rule to express $d\theta_{eh}$ in terms of dr_{eh}:

$$d\theta_{eh} = \left(\frac{\partial r_{eh}}{\partial \theta_{eh}}\right)^{-1} dr_{eh} = \frac{r_{eh}}{r_e r_h \sin(\theta_{eh})}\, dr_{eh} \tag{A4}$$

Using the identity $\sin(x) = \sqrt{1 - \cos^2(x)}$ and the expression for $\cos(\theta_{eh})$ obtained from the law of cosines:

$$\cos(\theta_{eh}) = \frac{r_e^2 + r_h^2 - r_{eh}^2}{2r_e r_h},$$

we can write:

$$dA = 8\pi r_e r_h \cdot \frac{r_{eh}}{r_e r_h \sqrt{1 - \left(\frac{r_e^2 + r_h^2 - r_{eh}^2}{2r_e r_h}\right)^2}}\, dr_e\, dr_h\, dr_{eh}$$

$$= 8\pi \frac{r_e r_h r_{eh} dr_e dr_h dr_{eh}}{\sqrt{|[(r_e + r_h)^2 - r_{eh}^2][r_{eh}^2 - (r_e - r_h)^2]|}} \tag{A5}$$

2. 3D Sphere

For the 3D case, we wish to change from spherical coordinates to variables that depend on the positions of the electron and hole and their relative distance, that is,$(r_e, \theta_e, \phi_e, r_h, \theta_h, \phi_h) \longrightarrow (r_e, r_h, r_{eh})$. Due to the spherical symmetry of the problem, the angular dependence can be reduced to the relative angle between the radial vectors of the two particles, defined as θ_{eh}. The differential element in spherical coordinates becomes:

$$d\tau = 8\pi^2 r_e^2 r_h^2 \sin(\theta_{eh})\, dr_e\, dr_h\, d\theta_{eh} \tag{A6}$$

Using the law of cosines:

$$r_{eh}^2 = r_e^2 + r_h^2 - 2r_e r_h \cos(\theta_{eh}) \tag{A7}$$

To change variables from θ_{eh} to r_{eh}, we use the Jacobian derived from expression (A4). Substituting into the differential volume element:

$$d\tau = 8\pi^2 r_e^2 r_h^2 \sin(\theta_{eh}) \cdot \frac{r_{eh}}{r_e r_h \sin(\theta_{eh})}\, dr_e\, dr_h\, dr_{eh}$$

$$= 8\pi^2 r_e r_h r_{eh}\, dr_e\, dr_h\, dr_{eh} \tag{A8}$$

Appendix B: Integrand of $\hat{H}_D$

As explained and shown in Eq. 7, the integrand of the kinetic energy operator for the electron is given by the scalar product $(\vec{\nabla}_e \Phi) \cdot (\vec{\nabla}_e \Phi)$,, the case for the hole is analogous.

Handling the scalar product is more straightforward in in-plane Cartesian coordinates. These coordinates are related to the set $\{r_e, r_h, r_{eh}\}$ through the following transformation:

$$r_e = \sqrt{x_e^2 + y_e^2},\ r_h = \sqrt{x_h^2 + y_h^2},\ \vec{r_e} \cdot \vec{r_h} = x_e x_h - y_e y_h$$

$$r_{eh} = \sqrt{r_e^2 + r_h^2 - 2\vec{r_e} \cdot \vec{r_h}} = \sqrt{(x_e - x_h)^2 + (y_e - y_h)^2} \tag{B1}$$

where the scalar product comes from the expression $\vec{r_e} \cdot \vec{r_h} = r_e r_h \cos(\theta_{eh})$. Performing the scalar product:

$$(\vec{\nabla}_e \Phi) \cdot (\vec{\nabla}_e \Phi) = \left(\frac{\partial \Phi}{\partial x_e}, \frac{\partial \Phi}{\partial y_e}\right) \cdot \left(\frac{\partial \Phi}{\partial x_e}, \frac{\partial \Phi}{\partial y_e}\right) =$$

$$= \left(\frac{\partial \Phi}{\partial x_e}\right)^2 + \left(\frac{\partial \Phi}{\partial y_e}\right)^2 \tag{B2}$$

Applying the chain rule to each partial derivative:

$$\frac{\partial \Phi}{\partial x_e} = \frac{\partial \Phi}{\partial r_e}\frac{\partial r_e}{\partial x_e} + \frac{\partial \Phi}{\partial r_{eh}}\frac{\partial r_{eh}}{\partial x_e} = \frac{x_e}{r_e}\frac{\partial \Phi}{\partial r_e} + \frac{x_e - x_h}{r_{eh}}\frac{\partial \Phi}{\partial r_{eh}} \tag{B3}$$

$$\frac{\partial \Phi}{\partial y_e} = \frac{\partial \Phi}{\partial r_e}\frac{\partial r_e}{\partial y_e} + \frac{\partial \Phi}{\partial r_{eh}}\frac{\partial r_{eh}}{\partial x_e} = \frac{y_e}{r_e}\frac{\partial \Phi}{\partial r_e} + \frac{y_e - y_h}{r_{eh}}\frac{\partial \Phi}{\partial r_{eh}} \tag{B4}$$

Therefore, by straightforward calculation:

$$(\vec{\nabla}_e \Phi) \cdot (\vec{\nabla}_e \Phi) = \frac{x_e^2}{r_e^2}\left(\frac{\partial \Phi}{\partial r_e}\right)^2 + \frac{(x_e - x_h)^2}{r_{eh}^2}\left(\frac{\partial \Phi}{\partial r_{eh}}\right)^2 +$$

$$+ \frac{2x_e(x_e - x_h)}{r_e r_{eh}}\left(\frac{\partial \Phi}{\partial r_e}\right)\left(\frac{\partial \Phi}{\partial r_{eh}}\right) + \frac{y_e^2}{r_e^2}\left(\frac{\partial \Phi}{\partial r_e}\right)^2 +$$

$$+ \frac{(y_e - y_h)^2}{r_{eh}^2}\left(\frac{\partial \Phi}{\partial r_{eh}}\right)^2 + \frac{2y_e(y_e - y_h)}{r_e r_{eh}}\left(\frac{\partial \Phi}{\partial r_e}\right)\left(\frac{\partial \Phi}{\partial r_{eh}}\right) =$$

$$= \left(\frac{\partial \Phi}{\partial r_e}\right)^2 + \left(\frac{\partial \Phi}{\partial r_{eh}}\right)^2 + 2\frac{r_e^2 - \vec{r_e} \cdot \vec{r_h}}{r_e r_{eh}}\left(\frac{\partial \Phi}{\partial r_e}\right)\left(\frac{\partial \Phi}{\partial r_{eh}}\right) =$$

$$= \left(\frac{\partial \Phi}{\partial r_e}\right)^2 + \left(\frac{\partial \Phi}{\partial r_{eh}}\right)^2 + \frac{r_e^2 - r_h^2 + r_{eh}^2}{r_e r_{eh}}\left(\frac{\partial \Phi}{\partial r_e}\right)\left(\frac{\partial \Phi}{\partial r_{eh}}\right) \tag{B5}$$

Appendix C: Exact solutions

1. Bessel solution

When a system exhibits cylindrical symmetry, the Schrödinger equation in polar coordinates (r, θ) in the plane takes the form:

$$\left[\frac{1}{r}\frac{d}{dr}\left(r\frac{d}{dr}\right) + \frac{1}{r^2}\frac{d^2}{d\theta^2} + \frac{2mE}{\hbar^2}\right]\Phi(r,\theta) = 0 \tag{C1}$$

By applying separation of variables, that is, assuming a solution of the form $\Phi(r, \theta) = R(r)\Theta(\theta)$, we obtain a differential equation for the radial part:

$$r^2\frac{d^2R}{dr^2} + r\frac{dR}{dr} + (k^2r^2 - m^2)R = 0 \tag{C2}$$

This is the Bessel differential equation, whose regular solution at the origin is:

$$R(r) = J_m(kr) \tag{C3}$$

where J_m is the Bessel function of the first kind of order m. For the ground state (no angular momentum), we take $m = 0$, yielding:

$$R(r) = J_0(kr) \tag{C4}$$

Since the system is infinitely confined at the boundary of the cylinder, i.e., at $r = R$, the wavefunction must vanish there:

$$J_0(kR) = 0 \quad \Rightarrow \quad k = \frac{\theta_0}{R} \tag{C5}$$

where θ_0 is the first zero of the function J_0. This ensures:

$$\Phi(r = R) = 0$$

analogous to the sine function vanishing at the boundary of a one-dimensional infinite square well.

2. Cosine solution

In the z-direction, the particle is assumed to be confined within a finite region of length H, centered at the origin. A natural choice for the wavefunction in this direction is:

$$\Phi_z(z) = \cos\left(\frac{\pi z}{H}\right) \tag{C6}$$

This function vanishes at the boundaries $z = \pm\frac{H}{2}$, satisfying the condition:

$$\Phi_z\left(\pm\frac{H}{2}\right) = \cos\left(\frac{\pi}{2}\right) = 0,$$

which is consistent with the ground state of a particle in a one-dimensional infinite square well of width H.

The choice of a cosine function, rather than a sine, arises naturally when the well is symmetric around the origin. This ensures that the wavefunction is even in z, a desirable property for the ground state in symmetric potentials.

Appendix D: Wolfram Mathematica

In this section, we present the Mathematica codes used to perform the numerical evaluation of the integrals corresponding to the in-plane and z-direction components of the wavefunction.

These integrals are embedded within `FindMinimum` routines in order to determine the optimal value of the variational parameter α that minimizes the total energy of the system.

We also include `Do` loops that systematically iterate over different values of the cylinder radius R, allowing us to study the dependence of the energy on the lateral confinement size. This setup provides a variational framework for exploring the ground state energy as a function of geometric and variational parameters.

```
aux = {};
energy[alpha_?NumericQ] := (
  A = alpha;

  integralNumDisco = NIntegrate[
    disc, {re, 0, R}, {rh, 0, R}, {reh, Abs[re - rh],
        re + rh},
    AccuracyGoal -> 5, WorkingPrecision -> 10];

  integralCoul = NIntegrate[
    couldisc, {re, 0, R}, {rh, 0, R}, {reh, Abs[re - rh
        ], re + rh},
    AccuracyGoal -> 5, WorkingPrecision -> 10];

  integralNorDisco = NIntegrate[
    nordisc, {re, 0, R}, {rh, 0, R}, {reh, Abs[re - rh
        ], re + rh},
    AccuracyGoal -> 5, WorkingPrecision -> 10];

  integralDisco = integralNumDisco / integralNorDisco;

  integralcinz = NIntegrate[
    kinz, {ze, -H/2, H/2}, {zh, -H/2, H/2},
    AccuracyGoal -> 5, WorkingPrecision -> 10]/2;

  integralNorZ = NIntegrate[
    norz, {ze, -H/2, H/2}, {zh, -H/2, H/2},
    AccuracyGoal -> 5, WorkingPrecision -> 10];

  gc = -phiz^2 / ((-integralNorDisco/integralCoul) +
      Abs[ze - zh]);

  integralPotz = NIntegrate[
    gc, {ze, -H/2, H/2}, {zh, -H/2, H/2},
    AccuracyGoal -> 5, WorkingPrecision -> 10];

  integralZ = (integralcinz + integralPotz) /
      integralNorZ;

  integralTotal = integralZ + integralDisco
)

Do[
  R = r;
  values = FindMinimum[
    {energy[alpha]}, {alpha, 0.2, 2.5},
    Method -> {"PrincipalAxis", "PostProcess" -> False
        },
    MaxIterations -> 15, AccuracyGoal -> 5,
        PrecisionGoal -> 5,
    WorkingPrecision -> 10
  ];

  (* Store R, minimum energy, and optimal alpha *)
  AppendTo[aux, {R, values[[1]], values[[2, 1, 2]]}];
  Print[{R, values[[1]], values[[2, 1, 2]]}];
,
{r, Ri, Rf, pasoR}];
```